Available online at www.sciencedirect.com
ScienceDirect
ELSEVIER
Lithos 96 (2007) 225–242
LITHOS
www.elsevier.com/locate/lithos

Mantle contributions to crustal thickening during continental collision: Evidence from Cenozoic igneous rocks in southern Tibet

Xuanxue Mo [a,*], Zengqian Hou [b,*], Yaoling Niu [c], Guochen Dong [a], Xiaoming Qu [d], Zhidan Zhao [a], Zhiming Yang [d]

[a] *State Key Laboratory of Geological Processes and Mineral Resources and School of Earth Science and Mineral Resources, China University of Geosciences, Beijing 100083, China*
[b] *Institute of Geology, Chinese Academy of Geological Sciences, Beijing 100037, China*
[c] *Department of Earth Sciences, Durham University, Durham DH1 3LE, UK*
[d] *Institute of Mineral Resources, Chinese Academy of Geological Sciences, Beijing 100037, China*

Received 15 April 2006; accepted 24 October 2006
Available online 2 January 2007

Abstract

The Tibetan crust is twice as thick as average continental crust. Crustal compression and shortening as a result of Indian–Asian collision is often considered to be the primary cause for the crustal thickening. In this paper, we show that magmatic contribution is also important. We come to this conclusion by documenting the Paleogene Linzizong volcanic succession (LVS), its coeval granitoid batholiths and the Miocene adakitic rocks along the Gangdese magmatic belt in southern Tibet. It has been widely accepted that the Indian–Asian collision proceeded from a "soft" phase at ∼65–70 Ma to a "hard" phase at ∼45–40 Ma, followed by continued post-collisional convergence to the present. In response to the collision and post-collision convergence are a series of tectono-magmatic events recorded in the Gangdese magmatic belt. These include (1) the syn-collisional LVS volcanism (∼65–40 Ma) and the emplacement of southern Gangdese batholiths (a peak age of ∼50 Ma); (2) a period (∼40 Ma to 25 Ma) that is magmatically quiescent, yet tectonically dominated by active compression and crustal shortening; and (3) the emplacements of post-collisional adakitic rocks (∼25–12 Ma), potassic–ultrapotassic volcanics (∼25–10 Ma) and peraluminous muscovite-bearing granites (∼between 24 and 18 Ma). These three major events contribute in different ways to the crustal thickness. Phase I, formation of the lower juvenile crust from ∼65 Ma to 50 Ma with crustal thickening largely concentrated at ∼50–40 Ma via input of mantle-derived magmas; Phase II, crustal thickening by tectonic shortening at ∼40–25 Ma; and Phase III, retaining crustal thickness, but thinning of the lithospheric mantle since ∼25 Ma in response to crustal extension and upwelling and lateral flow of asthenospheric mantle. We emphasize that collision-induced crustal thickening took place mainly in the period of ∼50–40 Ma and ∼25 Ma, i.e., the period between the late stage of the LVS volcanism and the beginning of the adakitic rock emplacement. Most of the LVS rocks and the collision related granitoids in southern Gangdese have $\varepsilon_{Nd} > 0$, attesting to the significance of mantle input, most likely through re-melting of mantle-derived basaltic rocks, including the subducted Neo-Tethyan ocean crust. The petrologic and geochemical characteristics of the Miocene potassic adakitic rocks support the idea that the lower portion of the thickened Tibetan crust is mafic and is genetically associated with the earlier LVS magmatism. We estimate that the mantle material input contributed about 30% of the total thickness of the present-day Tibetan crust. By assuming a pre-collision crustal thickness of ∼35 km, then the tectonic contribution would be about 20 km.

Keywords: Crustal thickening; Indian–Asian collision; Juvenile crust; Input of mantle material; Tibet

* Corresponding authors.
E-mail addresses: moxx@cugb.edu.cn (X. Mo), hzq@cags.net.cn (Z. Hou).

0024-4937/$ - see front matter © 2006 Elsevier B.V. All rights reserved.
doi:10.1016/j.lithos.2006.10.005

1. Introduction

The Tibetan plateau has long been regarded as key to developing models of continental tectonics and mountain-building processes. The plateau is characterized by the thickest continental crust (60–80 km; Kind et al., 1996) on Earth with its deep portion being hot and soft (Zhao et al., 1997). However, how and when this thickened yet soft crust was formed is debatable. Most tectonic models concerning the evolution of the Tibetan plateau emphasize that Indian–Asian continental collision since the Paleocene exerted the primary control on crustal thickening by means of (1) Indian continental lithosphere subduction (Argand, 1924; Powell, 1986), (2) Indian continental crust impingement (Zhao and Morgen, 1987), and (3) collision-associated deformation (Dewey and Bird, 1970; England and Houseman, 1989). However, some authors (e.g., Ding and Lai, 2003) argued that the Tibetan crust was already thickened up to 50 km prior to the Indo–Asian collision in the Cretaceous. In all these models, the crust thickening is largely attributed to tectonic effects (cf. Zhao et al., 1997). However, as magmatism is known to play an important role in crust thickening along the Andes (Altherton and Perford, 1993; Schmitz, 1994; Petford and Atherton, 1996), it is necessary to evaluate mantle material contributions, including mantle-derived magmas, to crustal thickening along the Himalayan–Tibetan orogenic belt.

In this contribution, we do so by examining the significance of (1) the syn-collisional Linzizong volcanic succession (LVS), which is interpreted as a magmatic response to the Indian–Asian collision at ~65–40 Ma (Mo et al., 2003), and (2) the post-collisional adakitic rocks of mid-Miocene age (Hou et al., 2004) in the Gangdese range, southern Tibet.

2. Tectonic framework and structure of the crust of southern Tibet

The Himalayan–Tibetan orogen consists of several continental terranes accreted to the southern margin of the Asian continent since the Mesozoic (Fig. 1; Yin and Harrison, 2000). The Lhasa terrane, bounded by the Indus–Yarlung suture (IYS) in the south and the Bangong–Nujiang suture (BNS) to the north, was shortened by ~180 km in response to the collision and has a maximum crust thickness of ~80 km (Murphy et al., 1997). The Lhasa terrane underwent an Andean-type orogeny prior to the collision. The Neo-Tethyan plate subducted northwards beneath the Lhasa terrane during the Late Jurassic–Cretaceous, and formed several tectonic units, i.e., Indus–Yarlung suture zone, the Xigaze fore-arc basin (Durr, 1996), and the Gangdese arc granitoid batholiths (Schärer et al., 1984) along the southern margin of the terrane (Fig. 1). The Indian–Asian collision proceeded from a "soft" phase to a "hard" phase from ~65–70 Ma to ~45–40 Ma (Yin and

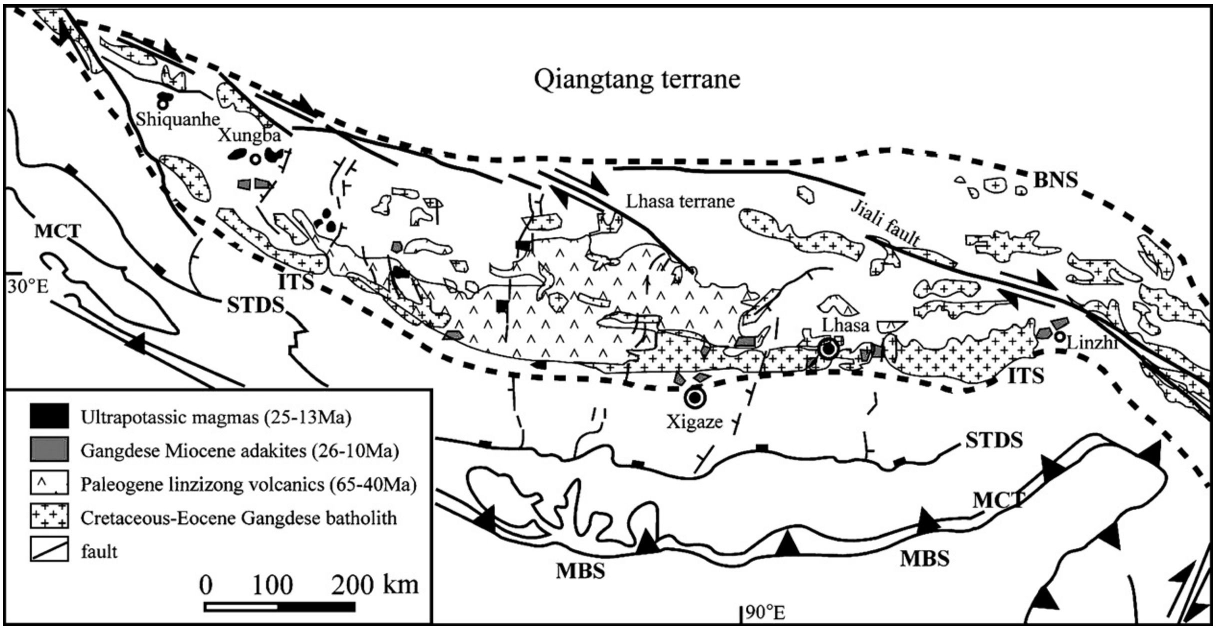

Fig. 1. Simplified geological map showing tectonic framework of the Tibetan orogenic belt and distribution of Cenozoic igneous rocks in Tibet (modified from Chung et al., 2003; Mo et al., 2003; Hou et al., 2004).

Harrison, 2000; Flower et al., 2001; Mo et al., 2003, and therein), followed by continued post-collisional convergence. Accordingly, a sequence of magmatic events took place and formed the ~2000-km-long, E–W-trending Gangdese magmatic belt. Collisional and post-collisional igneous rocks are mostly distributed in southern Gangdese and areally occupy 60% of the entire Gangdese magmatic belt. Temporally, the Gangdese magmatic belt consists of both syn-collisional (~65–40 Ma) and post-collisional (~25–10 Ma) igneous rocks with an intervening magmatic gap. The hard collisional phase also produced a major unconformity between strongly folded pre-Tertiary strata and the overlying Paleogene Linzizong volcanic succession (Mo et al., 2003). In addition, the initiation of east–west extension in southern Tibet may have occurred between 18 and 13 Ma, followed by an increase in deviatoric stress to initiate major normal faults between 9 and 5 Ma (Coleman and Hodges, 1995; Williams et al., 2001; Garzione et al., 2003; Kapp and Guynn, 2004). In central Tibet, estimates for normal-fault initiation are available only for the Shuang Hu rift from ca. 4 Ma (Yin et al., 1999) to ca. 14 Ma (Blinsiuk et al., 2001).

The INDEPTH II deep profiling results across southern Tibet (1992–1994) have confirmed the earlier seismological interpretations that the crust is 65–75 km thick (Molnar et al., 1998), reaching a maximum of 80 km beneath the Lhasa terrane (cf. Kind et al., 1996). This thickened crust (~70 km on average) is characterized by low seismic velocities (Vp=6 km/s, Vs=3.45 km/s). A ~20-km-thick low-velocity zone (Vs=3–3.1 km/s) and a ~14–20-km-thick high-velocity lower crust (Vp=7.2–7.5 km/s) have been recognized within this thickened crust in southern Tibet (Kind et al., 1996; Owens and Zandt, 1997). While the low-velocity zone was interpreted as a partially molten layer developed in the middle crust (Nelson et al., 1996), the high-velocity layer is most likely high-pressure garnet-bearing mafic rocks with a density >3.0 g/cm^3 at depth >~60 km (Owens and Zandt, 1997). The high density at the basal ~20 km is best interpreted as the presence of a mafic cumulate probably associated with the underplating of mantle-derived magmas or a layer of eclogitic rocks, depending on the thermal gradient. Moreover, available geophysical data indicate that the crustal thickness varies between ~60 km and ~80 km discontinuously in the east–west direction (Zhang, 2005).

3. Collisional and post-collisional magmatic events

During the period of Indian–Asian collision, the widespread 5-km-thick Linzizong volcanic succession (LVS), and the huge-scale granitoid batholiths formed in the south Gangdese terrane (Mo et al., 2003; references here). The sub-horizontal subaerial LVS overlies unconformably strongly folded Upper Cretaceous or even older marine strata. The $^{40}Ar/^{39}Ar$ age data on the LVS from the Linzhou Basin, in combination with regional data, indicate that the LVS eruption lasted for ~25 My (from ~65 Ma to ~40 Ma; Zhou et al., 2004). Overall, the Linzizong Volcanics broadly resemble average compositions of continental crust (Rudnick and Fountain, 1995), and hence contain useful information about magmatic contributions to continental crust growth genetically associated with continental collision.

Granitoids are mainly composed of granodiorite, quartz diorite, quartz monzonite and monzogranite, containing abundant mafic microgranular enclaves (MME). There are also small mafic intrusions associated with the granitoid batholiths. Field observations and systematic U–Pb SHRIMP dating show that the granitoid host, MMEs and mafic intrusives are essentially coeval (~47–52 Ma with the peak at ~50 Ma) (Schärer et al., 1984; Mo et al., 2005a; Dong et al., 2005). Furthermore, all these lithologies have ε_{Nd} $(t)>0$ (+2.34–+8.26), resembling the least contaminated rocks of the LVS. These characteristics all point to significant mantle contributions to crustal growth in southern Tibetan (Mo et al., 2005b).

After a quiescent period of ~15 My (i.e., 40–25 Ma), three types of post-collisional magmatism took place in large part simultaneously, from ~25 Ma to ~10 Ma in southern Gangdese (Fig. 1). These include (1) adakitic rocks emplaced during 25–12 Ma with a peak at 16 Ma; (2) a ~1300-km-long WNW−ESE belt (between 80°E and 91°E) of potassic–ultrapotassic volcanic rocks dated 25–10 Ma and generally becoming younger towards the east; and (3) some peraluminous granites of 24–18 Ma.

Chung et al. (2003) and Hou et al. (2004) interpreted the adakitic rocks as derived from partial melts of the thickened lower crust. The petrogenesis of the potassic–ultrapotassic volcanic rocks may be rather complex, involving partial melting of subducted Indian asthenospheric mantle, Tethyan ocean crust, terrigenous sediments, metasomatized Tibetan lithosphere and crustal level assimilation (Turner et al., 1993; Deng, 1998; Miller et al., 1999; Williams et al., 2001; Ding et al., 2003; Mo et al., 2006). The young (~24–18 Ma) peraluminous granites in southern Gangdese seem to be coeval or overlapping with the leucogranites in the Himalayan terrane (mostly at ~20–10 Ma), and both suites are muscovite-bearing (vs. cordierite-bearing) granites, implying that they may have formed at conditions of relatively high pressure and low temperature of thickened upper–mid crust (Barharin, 1996; Sylvester, 1998).

In summary, collisional and post-collisional igneous rocks, especially the LVS and the potassic adakitic rocks in the Lhasa terrane of southern Tibet respectively point to a magmatic contribution to crustal growth in response to the Indian–Asian continental collision. The positive ε_{Nd} (t) values and low initial $^{87}Sr/^{86}Sr$ ratios of most of these igneous rocks support the significance of mantle contribution.

4. Early Tertiary Linzizong volcanic succession (LVS)

The LVS is widespreadly along much of the 1500-km-long Gangdese magmatic arc in the southern part of the Lhasa terrane, immediately north of the IYS (Fig. 1). It has a maximum thickness of ~5 km, overlies unconformably the strongly folded Upper Cretaceous and older marine sedimentary strata, and is overlain unconformably by Oligocene red beds, thus indicating a major episode of Early Tertiary volcanic eruption. The large regional-scale unconformity of the LVS over the Cretaceous strata implies a major tectonic event, which is interpreted to indicate the major phase of the Indian–Asian continental collision (Mo et al., 2003).

4.1. Lithologic units and ages

On the basis of detailed mapping in the Linzhou volcanic district, near Lhasa, the LVS is readily divided into three formations (Fig. 2), i.e., Dianzhong, Nianbo and Pana Formations respectively (Dong, 2002). The

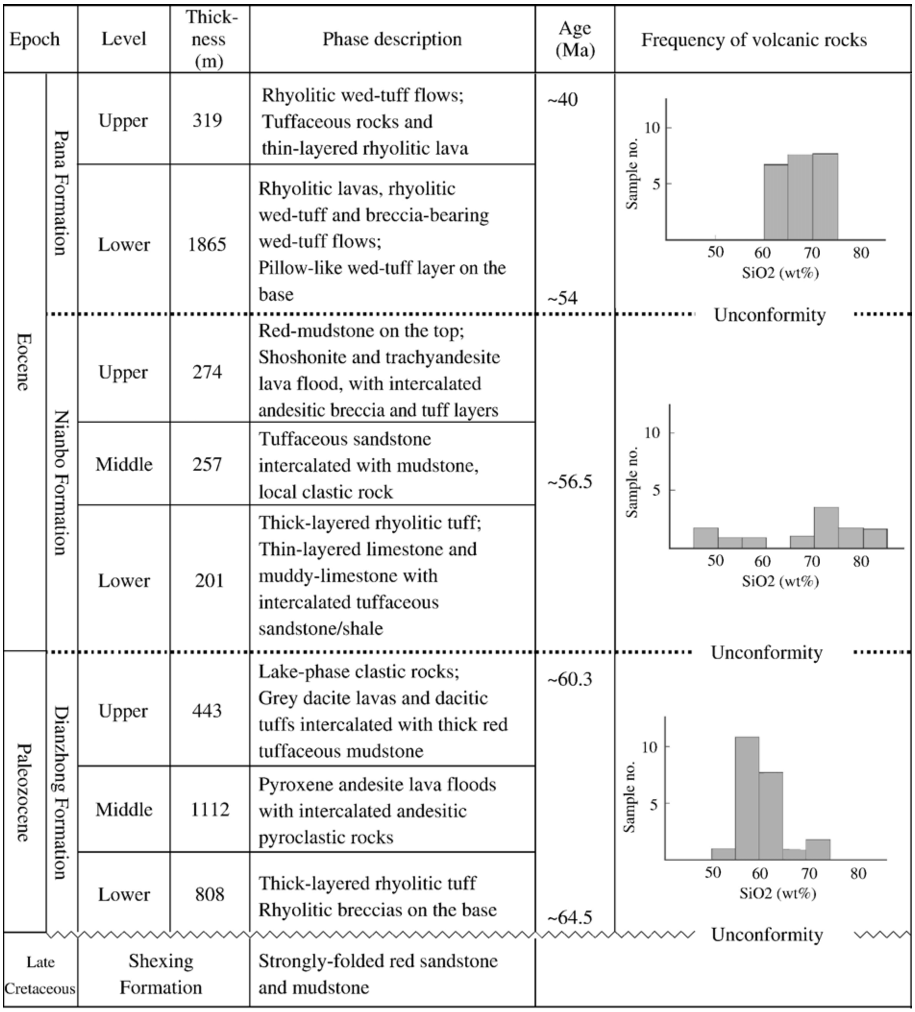

Fig. 2. Major lithologic units and dominant phases of the Linzizong volcanic succession in south Tibet.

2400-m-thick Dianzhong Formation consists of basal rhyolitic tuff unit, a middle andesitic lava unit, and an upper unit of andesitic tuff intercalated with red clastic rock, intruded by mafic dykes; the latter often contain plagioclase and clinopyroxene phenocrysts in a cryptocrystalline groundmass. The andesite lava flows dominate the formation, and have abundant phenocrysts (~15–30% plagioclase, ~5–15% pyroxene, ~5% amphibole, and minor biotite). $^{40}Ar/^{39}Ar$ dating on andesite and plagioclase from the Dianzhong volcanic rocks gives a plateau age ranging from 64.5 to 60.6 Ma (Maluski et al., 1982; Zhou et al., 2004). The ~700-m-thick Nianbo Formation comprises a 500-m-thick sedimentary sequence of limestone, muddy-limestone and tuffaceous sandstone/shale and a ~200-m-thick intercalary thin lava flows. Lithologically, volcanic rocks in the Nianbo Formation are rhyolitic lava/tuff and shoshonite-trachyandesite, and syn-volcanic dykes. The latter are potassic diabase and shoshonitic dykes, usually containing abundant amphibole and biotite phenocrysts in addition to plagioclase. Zhou et al. (2004) reported a $^{40}Ar/^{39}Ar$ plateau age of 56.5 Ma for the Nianbo olivine trachyandesite in the mid-position of the Formation. The Pana Formation is >2000 m thick, and is dominated by welded rhyolitic tuffs and lavas, intruded by syn-volcanic rhyolitic and shoshonitic dykes. The Pana Formation is conformably covered by lacustrine–facies sandy–mudstone (Fig. 2). $^{40}Ar/^{39}Ar$ dating gives an age range of ~50 to 40.8 Ma for the Pana rhyolitic rocks (Mo et al., 2003; Zhou et al., 2004).

4.2. Geochemistry of major and trace elements

Sixty-four samples from the LVS were analyzed for bulk-rock major elements by XRF and trace elements by ICP-MS at the Northwest University of China. Representative analyses and analytical procedures and uncertainties are given in Table 1.

Major element variation diagrams for LVS rocks show a large compositional range from basaltic to rhyolitic (Fig. 3). Although scattered, Al_2O_3, TiO_2, MgO, $Fe_2O_3^T$, CaO and P_2O_5 all show negative correlations with SiO_2 (Fig. 3). K_2O and Na_2O are more scattered, but a first-order positive K_2O–SiO_2 trend is apparent. On K_2O vs. SiO_2 plot, the Dianzhong and Nianbo volcanic rocks are mostly calc-alkaline, whereas the Pana volcanic rocks are high-K calc-alkaline with some being shonshonitic (Fig. 3a). Associated mafic dykes (44.3–51.6 wt.% SiO_2) range from calc-alkaline to shonshonitic, and have a considerable range of K_2O contents (0.8–2.9 wt.%) (Fig. 3a).

The LVS volcanic rocks all show LREE-enriched patterns with variable La_N/Yb_N ratios (7–24) and negative Eu anomalies (Fig. 4). The Dianzhong rocks show a range of La_N/Yb_N (7–15) and La/Sm (3. 8–6.2) ratios with no obvious Eu anomaly (Fig. 4a), suggesting that plagioclase involvement during magma generation and evolution is insignificant. The Nianbo shoshonite and basaltic trachyandensite show REE patterns similar to those of Dianzhong andesites, but Nianbo rhyolites show relatively high La_N/Yb_N (10–21) and La/Sm (5.2-6.5) ratios and an obvious Eu anomaly (Fig. 4b). The Pana rhyolitic rocks have the highest total REE contents and La/Sm ratios (6. 5–9.5), but similar La_N/Yb_N ratios (9–24) and Eu anomaly to those of the Nianbo rhyolites (Fig. 4c), suggesting the importance of plagioclase crystallization. The associated mafic dykes show similar REE patterns to the Dianzhong andesites and Nianbo shoshonite, but variable Eu anomalies (Fig. 4d).

The LVS volcanic rocks and associated mafic dykes exhibit similar primitive-mantle-normalized trace element patterns, with negative Nb, Ta, P, and Ti anomalies (Fig. 5a, b), suggesting that they may have shared a common parental magma or most likely were derived from a similar source by a similar process before they have evolved to different extents. The slightly different abundances levels among the three LVS formations could be explained by varying degrees of differentiation. These patterns resemble geochemical characteristics of 'arc-type' lavas (e.g., Tatsumi, 1986). The trace element patterns of the Pana rhyolites show similarity to the Miocene potassic and ultrapotassic lavas of the Lhasa terrane. It is noteworthy that all the LVS rocks have relatively high Y (>15 ppm) and Yb (>1.6 ppm), and low but variable La_N/Yb_N (7–24) and Sr/Y (<30) ratios, showing affinity with arc andesite–dacite–rhyolite association (Fig. 7), but different from the Miocene adakitic rocks in this terrane (see below).

4.3. Sr–Nd isotope geochemistry

Sr and Nd isotopic compositions of the LVS rocks were analyzed at the Institute of Geology and Geophysics, Chinese Academy of Sciences and analytical procedures and results were given in Table 2. The Nd and Sr isotopic compositions of the LVS rocks vary in relatively limited ranges in terms of $\varepsilon_{Nd}(t)$ (+3.29 to −3.96) and initial $^{87}Sr/^{86}Sr$ (0.704955 to 0.708316) (Fig. 6a). Fig. 6a plots our new data, in combination with those in the literature (Dong, 2002; Mo et al., 2003) in $\varepsilon_{Nd}(t)$–$(^{87}Sr/^{86}Sr)_i$ space. Most of the LVS rocks plot in a restricted field between the two mixing lines of 'Yarlung MORB–Lower Crust' and 'Yarlung MORB–

Table 1
Major and trace element abundances in the representative samples from the LVS, south Tibet

Formation	Dianzhong				Nianbo			Pana			Mafic dykes			
Sample No	BD-123	BD-126	BD137-2	Lz9913	Lz993	Lz991	N-9	Lz9914	BD-106	BD-114	BD-100	BD-72	BD-138	LZ9922
SiO_2	56.97	69.95	55.83	55.21	68.13	73.9	51.57	74.62	66.8	75.09	49.37	48.3	48.67	44.28
TiO_2	0.77	0.34	0.81	0.86	0.47	0.13	0.81	0.18	0.36	0.24	0.72	0.89	0.87	0.96
Al_2O_3	16.07	14.01	18.64	18.06	15.31	14.28	17.04	13.16	14.14	12.55	15.27	16.74	16.51	17.12
TFe_2O_3	6.73	3.13	6.63	8.3	3.25	1.68	8.53	1.29	3.19	1.47	8.29	9.13	9.48	9.82
FeO	2	1.5	2.4	2.85	0.4	0.4	1.95	1.3	0.65	0.2	3.7	3.88	5.38	5.18
MnO	0.1	0.08	0.1	0.14	0.04	0.02	0.1	0.02	0.11	0.08	0.24	0.19	0.15	0.15
MgO	2.3	1.04	2.1	4.01	1.62	1.05	3.46	0.08	0.7	0.34	5.08	3.62	3.9	3.33
CaO	5.35	1.77	7.07	7.29	1.76	0.95	7.89	0.41	3.09	0.46	6.54	6.86	8.32	11.44
Na_2O	4.76	4.48	3.95	2.98	0.95	0.55	3.9	3.57	2.45	3.23	3.46	3.81	2.28	2.18
K_2O	1.05	3.12	1.15	1.47	4.18	4	1.19	5.24	4.62	5.23	2.82	2.51	2.93	0.83
P_2O_5	0.2	0.07	0.25	0.22	0.1	0.03	0.43	0.06	0.15	0.05	0.22	0.37	0.37	0.39
LOI	5.72	1.93	3.32	1.3	4.5	3.54	5.01	1.1	3.93	1.42	7.58	7.57	6.43	9.52
Total	100.02	99.92	99.86	99.84	100.31	100.13	99.93	99.73	99.54	100.16	99.57	99.99	99.92	100.02
Ba	267	557	595	313	115	503	558	590	770	310	436	1224	806	633
Rb	34.5	92.7	23.2	36.8	144	132	24.6	185	151	167	72.5	59	72.2	22
Sr	377	249	656	477	87.2	86.1	1327	151	203	102	453	604	735	1086
Nb	6.7	10.2	7.26	4.92	10.35	9.52	10.2	5.51	13	22.4	5.38	10.4	9.64	12.9
Ta	0.46	0.76	0.41	0.51	1.13	1.07	0.46	1.08	0.95	1.77	0.33	0.45	0.41	0.68
Zr	183	181	182	149	160	113	162	119	176	213	112	143	133	107
Hf	4.27	4.96	4.65	3.92	5.95	4.97	3.88	4.1	4.51	6.08	2.86	3.51	3.28	2.51
U	1.34	2.63	1.31	1.26	3.86	3.43	2.36	6.09	5.48	8.52	1.93	2.08	2.15	2.4
Th	8.4	15.8	7.22	4.92	20.2	22.5	15.4	19.3	30	51.3	10.1	13.6	13.1	11.9
Y	21	27.8	29	22.7	19.3	21.5	24.8	4.61	21.6	26.7	23.5	27.5	28.5	28.8
Sc	18	8.43	18	18.1	9.29	7.41	12.1	0.73	6.63	5.15	26.6	18.1	19.5	17.4
Cs	1.84	1.24	3.13	0.66	19.46	7.65	1.38	4.29	6.09	2.15	3.69	11.3	0.71	7.5
La	21	32.5	23.7	18.2	32.8	36.9	47.1	13.2	39.8	31.8	22.8	45.6	46.1	53.6
Ce	41	62.8	50.8	45.4	64.8	74.8	86.9	38.9	72.2	105	43.8	87.7	84.3	113
Pr	5.06	7.24	6.45	5.23	7.84	9.21	10.6	2.68	7.94	6.67	5.28	10.6	10.7	12.8
Nd	20.6	27.4	27.3	22.5	28.2	33.3	42.6	8.71	28.6	23.2	21.8	43.2	44.5	52.8
Sm	4.43	5.48	6.06	4.39	5.25	6.43	8.23	1.48	5.41	4.71	4.91	9.02	9.15	9.57
Eu	1.22	1.22	1.64	1.28	0.73	0.6	2.07	0.32	1.15	0.59	1.32	2.2	2.25	2.38
Gd	4.33	5.44	5.92	4.36	4.15	5.1	7.85	1.13	5.35	5.3	5.07	8.45	8.88	8.12
Tb	0.65	0.8	0.89	0.72	0.61	0.75	0.95	0.16	0.72	0.78	0.74	1.09	1.14	1.23
Dy	3.73	4.8	5.04	4.14	4.03	4.86	4.85	0.99	4	4.87	4.37	5.72	5.78	5.97
Ho	0.76	0.98	1.01	0.82	0.83	0.97	0.86	0.21	0.79	1.05	0.92	1.02	1.04	1.06
Er	1.98	2.63	2.63	2.37	2.22	2.64	2.22	0.61	2.16	2.95	2.47	2.56	2.53	2.88
Tm	0.29	0.4	0.39	0.33	0.3	0.37	0.31	0.1	0.32	0.47	0.37	0.36	0.34	0.35
Yb	2.11	2.99	2.8	2.5	2.17	2.59	2.23	0.67	2.37	3.38	2.65	2.46	2.38	2.45
Lu	0.32	0.45	0.41	0.37	0.31	0.39	0.32	0.09	0.37	0.5	0.4	0.36	0.34	0.36
∑REE	201.38	287.54	249.10	201.24	274.32	313.46	403.87	115.29	319.89	315.65	221.45	407.41	409.52	476.39
δEu	1.00	0.89	0.99	1.02	0.79	0.64	0.96	1.00	0.87	0.63	0.96	0.96	0.94	1.02
$(La/Yb)_N$	6.73	7.35	5.72	4.92	10.21	9.63	14.27	13.31	11.35	6.36	5.81	12.53	13.09	14.78
Sr/Y	18.0	9.0	22.6	21.0	4.5	4.0	53.5	32.8	9.4	3.8	19.3	22.0	25.8	37.7
Y/Yb	10.0	9.3	10.4	9.1	8.9	8.3	11.1	6.9	9.1	7.9	8.9	11.2	12.0	11.8

Notes: geochemical composition of whole rocks was measured at the Key Laboratory of Continental Dynamics, Northwest University, China. Major element composition was analyzed by XRF (Rikagu RIX 2100) using fused glass disks. Trace element composition was analyzed by ICP-MS (Elan 6100 DRC) after acid digestion of samples in a Teflon bomb. They are also analyzed by XRF using powered pellets. Concentrations of Sr, Y, Nb, Zr, Cr and Ni obtained using these two methods for the same samples generally agree to within 10% errors. Analyses of rock standards (AGV-1, GSR-01, and BCR-2) indicate precision and accuracy better than 5% for major elements and 10% for trace and rare earth elements.

Amdo Orthogneiss'. Herein the Yarlung MORB (Mahoney et al., 1998) is assumed to represent the Neo-Tethyan oceanic lithospheric mantle component and the Amdo Orthogneiss (Miller et al., 1999) to represent typical upper crust material in Tibet, respectively. The lower crustal values of $^{87}Sr/^{86}Sr$ and $^{143}Nd/^{144}Nd$ are cited from Ben Othman et al. (1984). The Nianbo rocks (($^{87}Sr/^{86}Sr)_i$ 0.706871 to 0.708316,

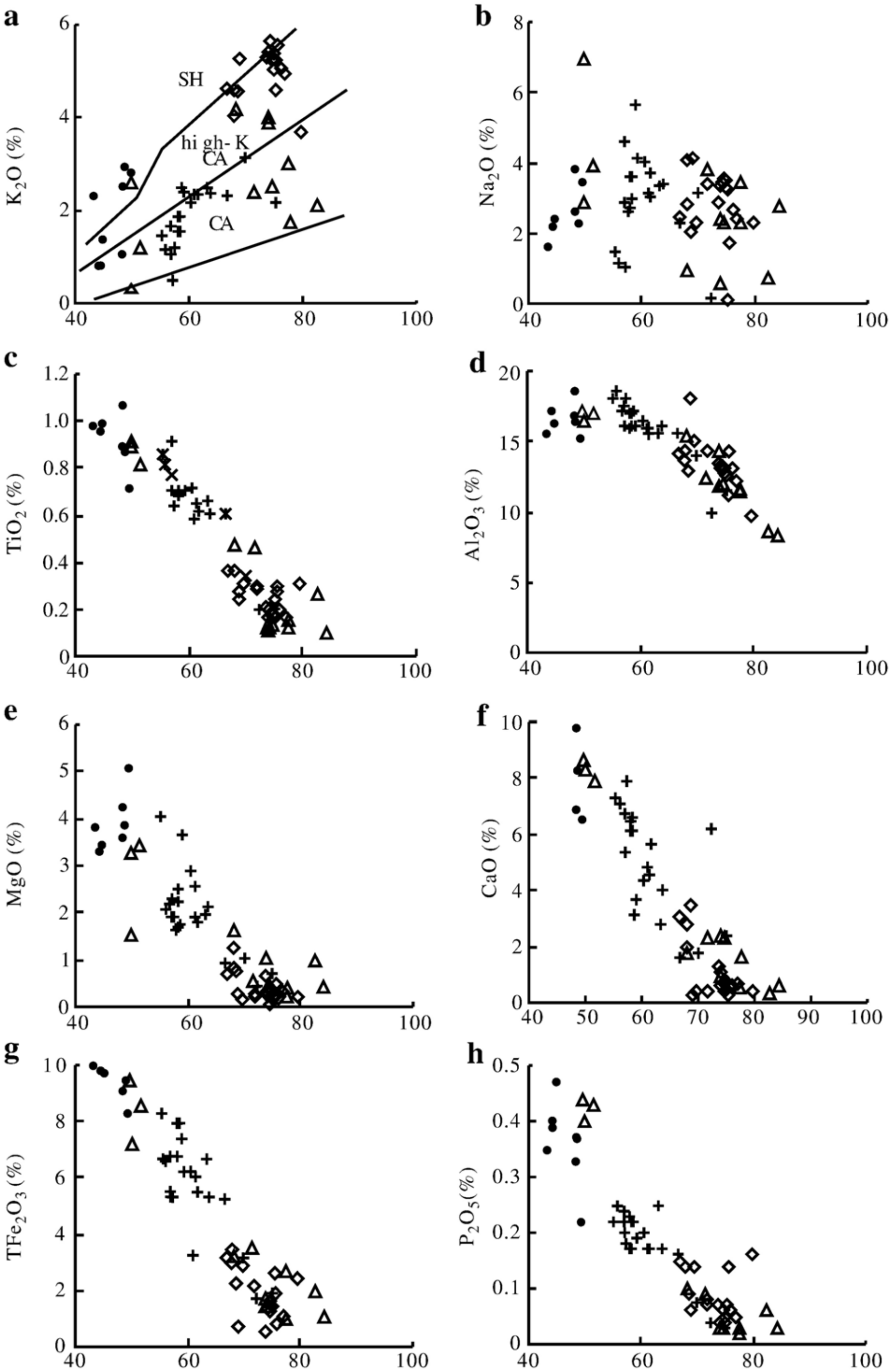

Fig. 3. Harker diagram for major elements in rocks from the LVS. E_{1d}: Dianzhong volcanic rocks (+); E_{2n}: Nianbo volcanic rocks (△); E_{2p}: Pana volcanic rocks (◇); mafic dikes (●).

ε_{Nd} (t) +0.39 to −3.96) distribute near the mixing line of Yarlung MORB–Amdo Orthogneiss, implying more upper-crustal contamination. The Pana rocks (($^{87}Sr/^{86}Sr)_i$ 0.704957 to 0.705692, ε_{Nd} (t) +0.77–+5.43) distribute closer to the mixing line of Yarlung MORB–Lower Crust, suggesting more low-crustal contribution. Within

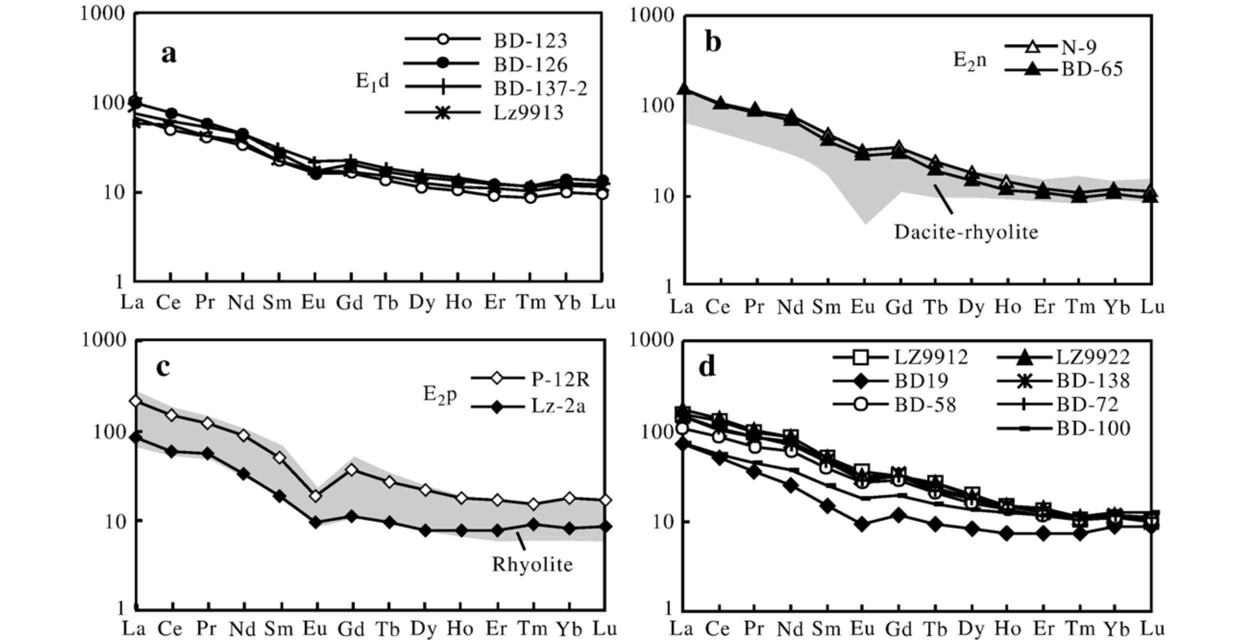

Fig. 4. REE patterns of the representative rock samples from the LVS. (a) the Dianzhong Formation, (b) Nianbo Formation, (c) Pana Formation, (d) associated mafic dykes.

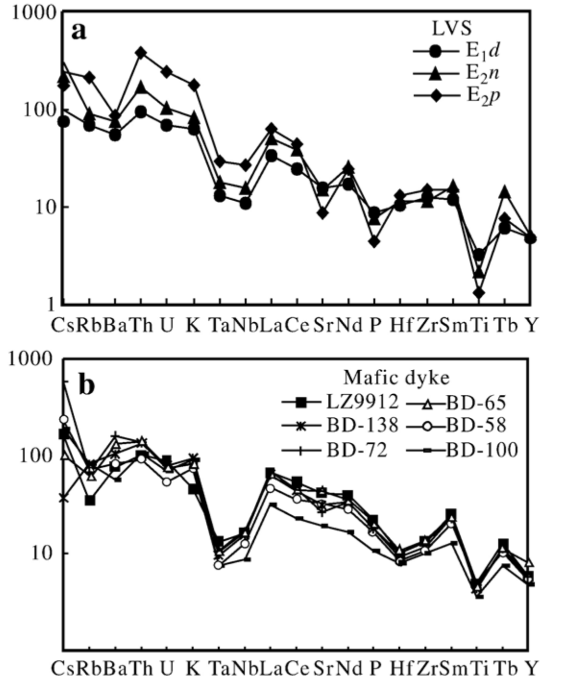

Fig. 5. Normalized abundance patterns of trace elements by primitive mantle (Mcdonough et al., 1991) for representative rock samples from the LVS. (a) Rocks from the LVS: E_{1d}: Dianzhong Formation; E_{2n}: Nianbo Formation; E_{2p}: Pana Formation, (b) associated mafic dykes.

the data set, the mafic dykes with ε_{Nd} (t) +3.29 and $(^{87}Sr/^{86}Sr)_i$ 0.704955 are the most primitive rock available in the area, and may represent isotopically the least contaminated mantle-derived melt parental to the LVS in terms of ultimate source materials.

5. Mid-Miocene adakitic rocks

The mid-Miocene is another major period of Cenozoic magmatism in the Lhasa terrane. The magmatism occurred spatially within the Linzizong volcanic belt along the IYS (Fig. 1), forming a 1300-km-long post-collisional magmatic belt. This belt extends westwards to the Neogene potassic magmatic belt in the South Karakorum (Maheo et al., 2002), and is bounded to the east by a large-scale strike–slip fault zone and NW-directed Paleocene potassic magmatic belt in eastern Tibet (Chung et al., 1998; Hou et al., 2003). We consider the Miocene magmatic belt to represent a significant thermal event after termination of the LVS volcanism ~40 Ma.

In this magmatic belt, adakitic rocks, occurring mainly as stocks and minor lavas, are spatially and temporally associated with the Miocene potassic and ultrapotassic rocks. The adakitic stocks mostly intrude the Gangdese granitoid batholiths, and genetically give

Table 2
Sr–Nd isotope compositions of the representative samples from the LVS, south Tibet

Sample no.	Locality	Formation	Rb (ppm)	Sr (ppm)	$^{87}Rb/^{86}Sr$	$^{87}Sr/^{86}Sr$	$^{87}Sr/^{87}Sr(i)$	Sm (ppm)	Nd (ppm)	$^{147}Sm/^{144}Nd$	$^{143}Nd/^{144}Nd$	ε_{Nd} (*t*)	NCI
Lz9915	Linzhou	Pana	148.2	360.4	1.19	0.705718±9	0.704957	5.188	29.14	0.1077	0.512665±11	1.04	0.28
Lz9914	Linzhou	Pana	183.2	184.9	2.868	0.707123±25	0.705290	2.271	12.88	0.1067	0.512651±5	0.77	0.29
L1087–2	Linzhou	Pana	177.53	188.4	2.721	0.707431±15	0.705692	2.741	15.871	0.1044	0.512889±9	5.43	0.16
Lz991	Linzhou	Nianbo	147.6	92.3	4.625	0.710485±13	0.706871	5.802	30.4	0.1154	0.512633±9	0.47	0.3
Lz993	Linzhou	Nianbo	165.4	97.06	4.936	0.711575±18	0.707718	4.683	26.19	0.1082	0.512626±13	0.39	0.31
LZ998	Linzhou	Nianbo	92.91	57.51	4.678	0.711971±10	0.708316	2.833	14.38	0.1192	0.512407±7	-3.96	0.47
Lz9913	Linzhou	Dianzhong	35.66	486.5	0.212	0.705176±11	0.704980	4.514	20.6	0.1325	0.512628±17	0.34	0.31
Lz9930	Linzhou	Dianzhong	52.44	390.1	0.3891	0.705671±12	0.705312	3.945	18.61	0.1282	0.512582±16	-0.52	0.34
Lz9924	Linzhou	Dianzhong	65.58	355.7	0.5336	0.705883±13	0.705390	4.273	21.46	0.1204	0.512583±10	-0.44	0.34
Lz9922	Linzhou	mafic dike	21.02	1100	0.05533	0.705002±11	0.704955	9.593	47.73	0.1216	0.512777±10	3.29	0.17

Notes: (1) Rb–Sr and Sm–Nd isotopic compositions were measured on a VG354 mass spectrometer at the Institute of Geology and Geophysics, Chinese Academy of Sciences. Whole-rock powders (70–50 mg) were dissolved for 7 days using a mixed acid ($HF:HClO_4=3:1$) in Teflon bombs, and isotopes were separated by AG50WX8 (H^+) exchangeable ion poles. Analyses of NBS987 standard run during the same period gave $^{87}Sr/^{86}Sr=0.710214\pm11$ ($N=10$). Analyses of BCR-1 and La Jolla Nd standard were measured as $^{143}Nd/^{144}Nd=0.512602\pm10$ and 0.511841 ± 9 ($N=12$), respectively. All measured $^{143}Nd/^{144}Nd$ and $^{86}Sr/^{88}Sr$ ratios are fractionation corrected to $^{143}Nd/^{144}Nd=0.7219$ and $^{86}Sr/^{88}Sr=0.1194$, respectively. (2) NCI refers to the Neodymium Crustal Index proposed by Depaolo (1985) and Depaolo et al. (1992), describing the fraction of crustal Nd in a rock. $NCI=[\varepsilon_{Nd}\ (rock)-\varepsilon_{Nd}\ (M)]/[\varepsilon_{Nd}\ (C)-\varepsilon_{Nd}\ (M)]$. (3) The calculation of $(^{87}Sr/^{86}Sr)_I$ and ε_{Nd} (*t*): $(^{87}Sr/^{86}Sr)_i=(^{87}Sr/^{86}Sr)_{rock}-(^{87}Rb/^{86}Sr)_{rock}*(e^{\lambda t}-1)$, where $\lambda=1.42*10^{-11}$; $\varepsilon_{Nd}\ (t)=[(^{143}Nd/^{144}Nd)_{rock,t}/(^{143}Nd/^{144}Nd)_{CHUR,t}-1]*10{,}000$, where $(^{143}Nd/^{144}Nd)_{CHUR,t}=(^{143}Nd/^{144}Nd)_{CHUR,present}-(^{147}Sm/^{144}Nd)_{CHUR,present}*(e^{\lambda t}-1)$, $(^{143}Nd/^{144}Nd)_{CHUR,present}=0.512638$, $(^{147}Sm/^{144}Nd)_{CHUR,present}=0.1967$, $\lambda_{Sm}=6.54*10^{-12}$, and $(^{143}Nd/^{144}Nd)_{rock,t}=(^{143}Nd/^{144}Nd)_{rock,present}-(^{147}Sm/^{144}Nd)_{rock,present}*(e^{\lambda t}-1)$.

rise to the 350-km-long Cu porphyry belt in the Lhasa terrane (Hou et al., 2004; Fig. 1). The corresponding volcanic rocks are preserved in Maquiang (Coulon et al., 1986) and Gazacun (Zhao et al., 2001), ~100 km west of Lhasa, and in S Gegar and SE Barga in western Gangdese (Miller et al., 1999). Available age data indicate that the magmatism took place in the period of 25–12 Ma with a peak at ~16 Ma for the adakitic intrusives and volcanics in southern Tibet (Coulon et al., 1986; Miller et al., 1999; Zhao et al., 2001; Chung et al., 2003; Qu et al., 2003; Hou et al., 2003, 2004; Rui et al., 2004). This age distribution suggests that the adakitic magmatism may be associated with the east–west extension, the exhumation of the Gangdese batholiths in 18–21 Ma (Copeland et al., 1995), and the molasses deposition in 19–20 Ma (Harrison et al., 1992) in response to the post-collisional crustal extension.

Chemical and isotope compositions of the adakitic rocks in southern Tibet have been reported by Hou et al. (2004) and Chung et al. (2003). Their petrographic and geochemical signatures are summarized here. The adakitic rocks are mainly porphyric monzogranite, quartz monzogranite and monzonite with 64.2-72.4 wt.% SiO_2. The adakitic volcanic rocks are dacite and dacitic–rhyolite. They are geochemically shoshonitic, and/or potassic calc-alkaline, with higher K_2O contents (2.6–8.7%) than those of Na-rich adakites produced from slab melting (Defant and Drummond, 1990; Defant and Kepezhinskas, 2001). These adakitic rocks are enriched in large-ion incompatible elements (LILE), and strongly depleted in high-field strength elements (HFSE: Nb, Ta, P, Ti). They have low abundances of Yb (0. 9–1.9 ppm) and Y (2. 9–8.0 ppm) with LREE-enriched patterns but no Eu anomaly, thus resulting in high La_N/Yb_N (12-40) and Sr/Y (30–175) values, similar to typical adakites derived from slab melting (Fig. 7). Their high La_N/Yb_N and Sr/Y ratios have been interpreted as partial melting of a garnet-bearing lithology (e.g., garnet amphibolite) with variable amount of garnet (10–30%) as a residual phase (Fig. 7). Their higher Rb/Sr (>0.1) and lower Nb/U ratios (<5) than those of most Cenozoic adakite and Archean adakite and high-Al TTG (Drummond et al., 1996) imply a large contribution of a lower-crustal source to the generation of the adakitic rocks in southern Tibet (Hou et al., 2004).

The adakitic intrusives show a relatively wide range of ε_{Nd} (*t*) (+2.3 to −6.2) and $(^{87}Sr/^{86}Sr)_i$ (0.7050 to 0.7075) (Hou et al., 2004; Fig. 6b), which contrasts with adakites of slab melting (Kay, 1978; Kay et al., 1993; Stern and Kilian, 1996). The adakitic lavas have relatively low ε_{Nd} (*t*) (−7.1 to −9.5) and high $(^{87}Sr/^{86}Sr)_i$ (0.70903 to 0.70967), towards the spatially associated Miocene ultrapotassic lavas on ε_{Nd} (*t*) vs. $(^{87}Sr/^{86}Sr)_i$ diagram (Fig. 6b). Most adakitic rocks in southern Tibet fall near the mixing line between the lower crust and

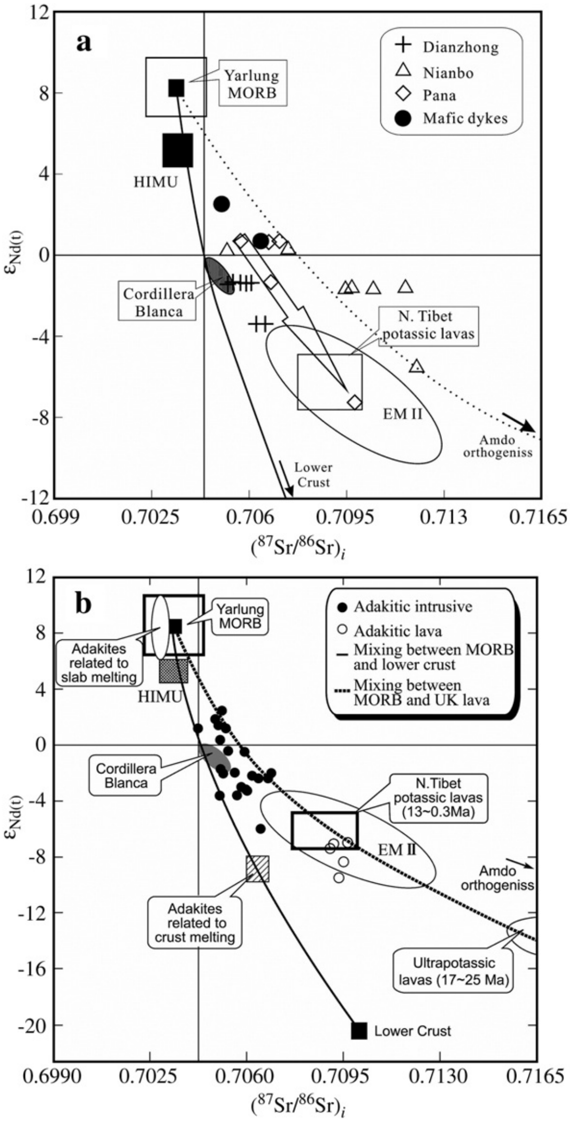

Fig. 6. $^{87}Sr/^{86}Sr$ versus ε_{Nd} (t) diagrams of LVS rocks (a) and Miocene adakitic rocks in southern Tibet (b). In a, Cenozoic volcanic rocks from northern Tibet and Yarlung MORB (Mahoney et al., 1998) were plotted for comparison. Most LVS rocks plot onto or near the mixing line between Yarlung MORB and northern Tibetan rocks. Some LVS rocks show distinct trends extending to upper crust (i.e., Amdo Orthogneiss; Miller et al., 1999) and lower crust (Ben Othman et al., 1984). In b, most adakitic rocks in southern Tibet are in the filed defined by mixing lines of depleted mantle (MORB) and with lower crust ($^{87}Sr/^{86}Sr = 0.7100$; $^{143}Nd/^{144}Nd = 0.5115$) and the Miocene ultrapotassic lavas in southern Tibet (Miller et al., 1999). Adakitic intrusives from the Cordillera Blanca (Petford and Atherton, 1996) and from crust melting in east China (Xu et al., 2002) were plotted for comparison. Data for adakites, derived from interpreted slab melting, on the Adak Island, Cook Island and Cerro Pampa (Kay, 1978; Kay et al., 1993; Stern and Kilian, 1996) are also plotted for comparison. DMM, HIMU and EMII represent three types of mantle end-members, respectively (Zindler and Hart, 1986).

Yarlung MORB (Mahoney et al., 1998) on ε_{Nd} (t) vs. $(^{87}Sr/^{86}Sr)_i$ diagram (Fig. 6b), which led Hou et al. (2004) to conclude that they were derived from partial melting of a hydrous, basaltic lower crust. Guo et al. (2007-this issue) also indicate a close correlation between the occurrence of post-collisional adakites and

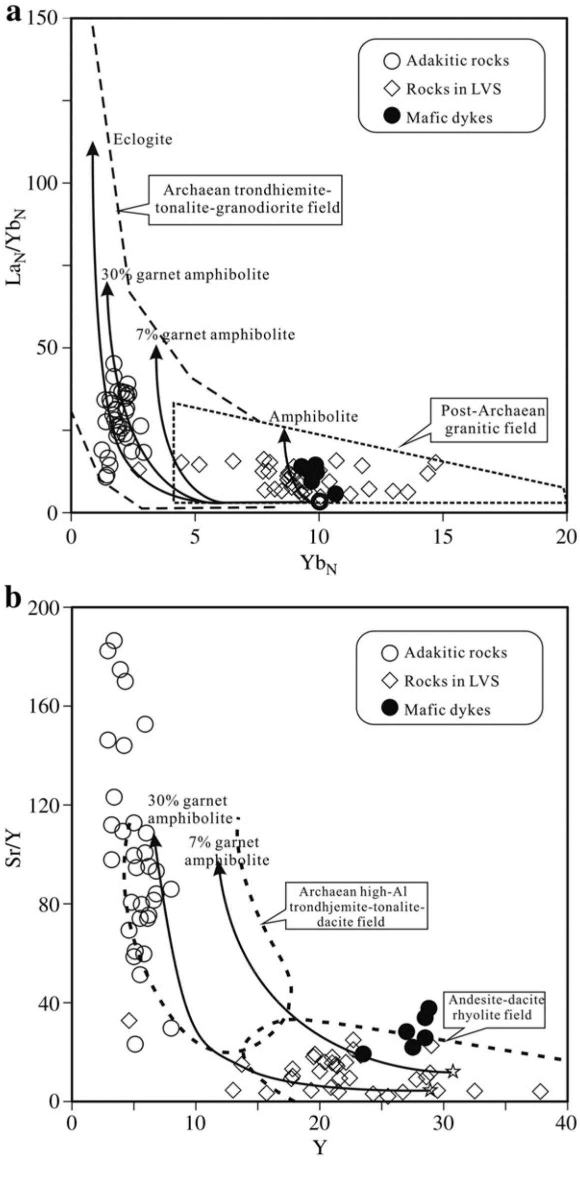

Fig. 7. (a) La_N/Yb_N vs. Yb_N (after Martin, 1986) and (b) Sr/Y vs. Y plots (Drummond and Defant, 1990), showing fields of adakites and arc intermediate-felsic rocks. Batch partial melting trends from a continental basalt source with variable phases from eclogite, garnet amphibolite to amphibolite are shown in a (Martin, 1986). Melting curves for two distinct sources with mineralogies of garnet amphibolite with 30% and 7% residual garnet are drawn in b (Petford and Atherton, 1996).

a series of N–S-trending rifts within the Lhasa terrane, and interpret the formation of adakites as a consequence of decompression melting of the lower crust.

6. Discussion

6.1. Input of the mantle material during the Indian–Asian collision (c.65–40 Ma)

As mentioned above, the LVS may be ideal for understanding the formation of juvenile crust and crustal thickening in response to the Indian–Asian collision. The spatial and temporal association of andesitic–dacitic–rhyolitic lavas with mafic dykes in the LVS suggests a genetic link between the felsic and mafic rocks. Their essentially identical trace element patterns (Fig. 5) suggest that they may share parental magmas with similar compositions or derived from a common source rock. The more felsic lithologies must have undergone complex evolution processes (e.g., assimilation and fractional crystallization process with contaminants of varying isotopic compositions) or alternatively, the more felsic lithologies may have derived by partial melting of the more mafic lithologies, which may have in turn been derived ultimately from the same mantle source. The latter is more likely because of the difficulty in producing volumetrically significant felsic melts by mantle melting and magma differentiation (e.g., the problem of "granitization"). The depletion in HFSE (Nb, Ta, Hf, P, Ti) and enrichment in LILE (Rb, Ba, K) for the LVS and associated mafic dykes (Fig. 5) resemble signatures of arc lavas, but such signatures can also be produced by partial melting of amphibolite with accessory ilmenite, in which the residual amphibole and in particular ilmenite would hold HFSEs, causing the apparent depletion of these elements. The enrichment of Sr (up to 1327 ppm) and the absence of significant Eu anomalies in most mafic rocks could be interpreted as melting a plagioclase-absent source rock, but it is also viable that partial melting may have eliminated plagioclase in the melting residue.

As elaborated above, partial melting of mantle peridotite cannot produce volumetrically significant felsic rocks. More mafic dykes are still far too evolved ($Mg^{\#}$, <0.62) to be primary mantle-derived magmas, but they are likely differentiated from the more primitive mantle-derived melts. Hence, the more felsic LVS rocks are unlikely direct melting products of mantle peridotite. The trace element similarity of the LVS rocks and the mafic dykes (Fig. 5) and their more mantle-like isotopic signatures (Fig. 6) (see below) suggest that all the LVS rocks (and perhaps the more mafic dykes as well) may have derived by partial melting of younger mantle-derived basaltic rocks. The recently subducted young Neo-Tethyan ocean crust would be ideal candidate. For example, the collision would retard subduction and thus facilitate thermal equilibration of the underthrust Neo-Tethyan ocean crust with the overlying asthenospheric "mantle wedge". Thus, this process would bring the ocean crust onto or above the amphibolite-solidus (Peacock, 2003), causing heating/compression (vs. decompression) hydrous melting (Niu, 2005) at a depth of <60 km. The resultant melts would be more felsic than peridotite-derived basaltic melts, but still possess mantle isotopic signatures. This suggests the mantle contribution to the mass of continental crust in response to the collision. Involvement of terrigenous sediments during subduction may explain the elevated abundances of K_2O in these rocks.

Fig. 6a shows that while some of the LVS rock samples possess mantle isotopic signatures (e.g., ε_{Nd} $(t)>0$), other samples deviate from the mantle composition towards isotopic signatures of the Tibetan upper crust (e.g., the Amdo Orthogneiss with low ε_{Nd} (t) and high $(^{87}Sr/^{86}Sr)_i$ or inferred lower continental crust (Ben Othman et al., 1984)). We interpret such deviation from the mantle signatures by some of the LVS rock samples as resulting from assimilation or contamination with existing crustal components, which are expressed in ε_{Nd} (t)–$(^{87}Sr/^{86}Sr)_i$ space as mixing trends. Details of these mixing processes/trends as well as the possible mantle end-member components of the Gangdese igneous rocks have been discussed elsewhere (Mo et al., 2006).

It is important to note that while the LVS major element trends in SiO_2 variation diagrams (Fig. 3) as well as trace elements systematics (Figs. 4–7) are qualitatively consistent with trends produced by fractional crystallization processes, the large age span (~20 Ma) suggests that these rocks are not linked by magma evolution from a common parental melt. Plot of La vs. La/Sm (Fig. 8) provides further information on the genetic relation among different LVS formations. The Dianzhong andesitic rocks exhibit an invariable HREE (Yb), but a wide range of LREE and LREE/HREE ratios, thus giving a trend paralleling to the anticipated partial melting trend on La–La/Sm diagram. This suggests that REEs of these andesitic melts record both melting and crystallization processes. Very low-degree hydrous melting of peridotite could produce andesitic melts, but to produce the observed volumes of felsic melts by peridotite melting is physically difficult and practically unlikely. Hence, the bulk of the LVS likely results from partial melting of a basaltic source

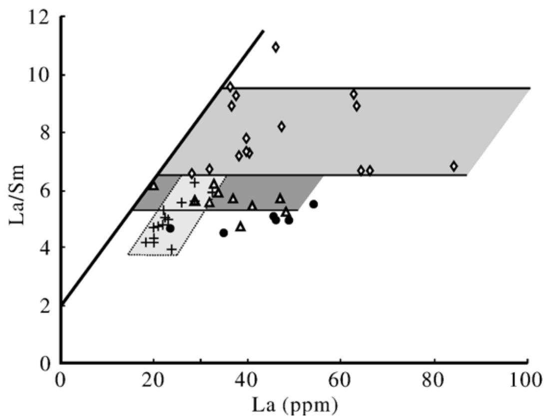

Fig. 8. La/Sm–La diagram illustrating partial melting trend and crystal fractionation trend for the rocks in the LVS, south Tibet. Symbols are the same as Fig. 3.

with subsequent fractional crystallization. Primitive mafic rocks resembling melt (vs. cumulate) compositions with $Mg^{\#}>0.7$ have not yet been observed, but the evolved mafic dykes with $Mg^{\#}$ values of 0.53–0.62 widely occur in the LVS. The varying $Mg^{\#}$ and La, yet relatively constant La/Sm seen in Fig. 8 for these dykes could be explained by varying extents of fractional crystallization or varying modal mineralogy. The origin and composition of "primary" melts parental to these dykes are unknown. They could be derived from metasomatized mantle peridotite or mantle peridotite with terrigenous sediment input. Alternatively, these dykes may in fact be melts of andesitic composition with abundant cumulus hydrous phases (e.g., amphiboles, biotite/etc.), giving rising to the SiO_2-poor bulk compositions.

For estimating the crustal/mantle contributions to the LVS, the Neodymium Crustal Index (NCI) proposed by Depaolo (1985), Depaolo et al. (1992) and Perry et al. (1993) was employed here (Table 2):

$$NCI = [\varepsilon Nd\ (rock) - \varepsilon Nd(M)]/[\varepsilon Nd(C) - \varepsilon Nd)(M)],$$

where M and C refer to the mantle and the crust respectively. This is a useful approach as it estimates mass contributions of crustal Nd in rocks experienced crustal assimilation during its evolution (Depaolo et al., 1992). As seen in Table 2, NCI for the entire LVS system ranges from 0.16 to 0.47 with 0.30 on average; those for mafic dykes, the Dianzhong, the Nianbo, and the Pana volcanics are 0.17, 0.31–0.34, 0.30–0.47 and 0.16–0.29, respectively. Obviously, in terms of Nd isotopes, the LVS and the associated dykes are dominated by mantle contributions, up to 70–84%. The "mantle" here refers to juvenile crust, which we interpreted as recently subducted Neo-Tethyan ocean crust probably associated with terrigenous sediments as discussed above. It is also inevitable that the crustal contributions to the LVS increased with advanced degrees of crustal level magma cooling and assimilation, especially as seen in the Nianbo volcanics.

6.2. Thickened juvenile lower crust: a possible source for the Miocene adakitic rocks in southern Tibet

Significant differences in major and trace elements and isotopic compositions indicate that the Miocene potassium-rich adakitic rocks in southern Tibet were derived from a source that differs from youthful subducted oceanic slab for generating sodium-rich adakites in arc settings (Hou et al., 2004). Abnormally high K_2O contents and relatively high $^{87}Sr/^{86}Sr$ (0.7050 to 0.7075) and low ε_{Nd} (+2.3 to −6.2) led Chung et al. (2003) and Hou et al. (2004) to conclude that these potassic adakitic rocks were generated by partial melting of a thickened basaltic lower-crust underneath southern Tibet. However, as suggested by Sr–Nd isotopic signatures of these adakitic rocks (see Fig. 6b), this thickened lower crust was juvenile and consisted prevailingly of mafic lithologies. The juvenile crust might be attributed to intense underplating or assimilation of (1) Miocene ultrapotassic and potassic magmas, erupted during 25–10 Ma (Turner et al., 1993; Miller et al., 1999; Mo et al., 2006), (2) Late Cretaceous arc basaltic magmas related to subduction of the Neo-Tethyan oceanic slab during 120–70 Ma, and (3) the Linzizong parental magmas (65–45Ma) related to Indian–Asian continental collision since Paleocene. With regard to case (1), available age data indicate that the ultrapotassic–potassic magmatism is coeval with adakitic rocks (25–12 Ma, Chung et al., 2003; Hou et al., 2003, 2004; Rui et al., 2004). It is thus unlikely that these ultrapotassic melts firstly assimilated the lower crust and then triggered the melting of the juvenile crust in such a short time. As for case (2), if arc magmas derived from a mantle wedge and underplated at the base of the lower crust during the subduction timeframe (i.e., 120–70 Ma), these magmas would have triggered lower-crust melting, but no such lower crust-derived igneous rocks, e.g., adakites, were found in pre-Miocene igneous suites in southern Tibet. It follows that underplating of mafic magmas related to the Neo-Tethyan subduction and subsequent Indian–Asian collision during c.65–40 Ma may have produced a thickened juvenile lower crust, from which adakitic magmas were derived in the Miocene. The hypothesis is supported by the following two lines of evidence.

The first evidence comes from the U–Pb ages of zircon crystals in the Miocene adakitic rocks. Two groups of zircons are recognized by distinct morphology (Fig. 9) and U–Pb ages (Fig. 10). The first group has well-developed crystal forms with typical rhythmic zoning. SHRIMP analysis indicates that these zircons are enriched in Y, Hf and P, and characterized by enrichment of HREE with negative Eu anomaly and high Th/U ratio (0.18–0.47; Qu et al., unpublished data). They yielded a range of U–Pb ages between 12 and 25 Ma with a peak at 16±5 Ma, representing the crystalline age of the adakitic rocks. The second group of zircons has complex features (e.g., residual nucleus, patch- or sponge-like; Fig. 9). They have relatively low Y (700–1600 ppm) and U (80–300 ppm; Qu et al., unpublished data), and thus plot in the field of mafic rocks on Y–U diagram (not shown), indicating that these residual zircons were crystallized from a mafic magma. U–Pb ages of these zircons range from 65 to 45 Ma, peaking at 55±10 Ma (Rui et al., 2004; Qu et al., unpublished data), coeval with that of the LVS (65–40 Ma). The bimodal distribution of zircon U–Pb ages indicates that the Miocene adakitic rocks (Fig. 10) were probably derived from a more mafic source with zircon U–Pb age of 55±10 Ma. No zircons with U–Pb ages >65 Ma have been observed, thus ruling out the possibility that the pre-collisional Neo-Tethyan subducted oceanic slab acted as a potential source for the Miocene adakitic rocks.

The similarities of Sr–Nd isotopes of the Miocene adakitic rocks to those of the LVS (Fig. 6a and b) further support the idea that newly formed more mafic crust could be an ideal source for adakitic melts in southern Tibet. Most adakitic porphyry intrusives and volcanic rocks have Sr ($^{87}Sr/^{86}Sr$, 0.7050 to 0.7075) and Nd (ε_{Nd} (t), +2.3 to −6.2) isotopes very similar to

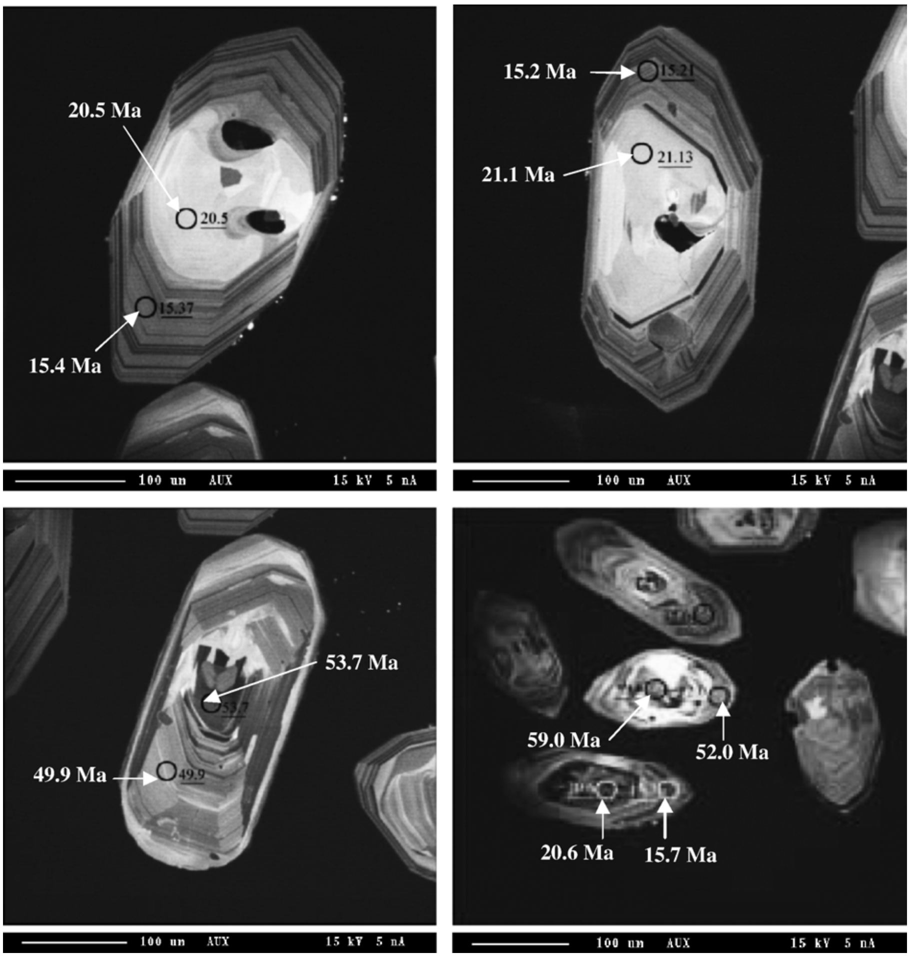

Fig. 9. Back-scattered electronic images of various zircon crystals in Miocene adakitic rocks from southern Tibet.

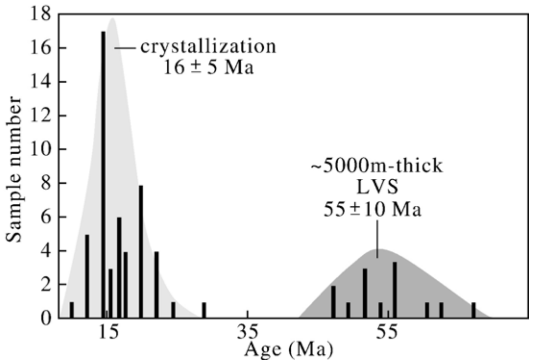

Fig. 10. Statistic distribution of zircon SHRIMP U–Pb ages for the Miocene adakitic rocks from southern Tibet. Note the distinct two age peaks at 16 Ma and 55 Ma, corresponding to the crystalline ages of igneous zircons from adakitic magmas and age of residual zircon in a source rocks that are temporarily equivalent to the main phase of the LVS (also granitoid batholiths) magmatism.

those of the LVS, especially the Dianzhong andesites and associated mafic dykes, suggesting a common ultimate mantle source.

Following the above arguments, we propose a two-stage model for the generation of the Miocene adakitic rocks. A similar model has been presented for the generation of the Cordillera Blanca batholith (Petford and Atherton, 1996). This model emphasizes that the input of mafic magmas originated from a hydrous mantle source with an enrichment of incompatible elements, forming the newly accreted basaltic lower crust during ~65–40 Ma. This lower portion of thickened crust was later partially melted in response to the upwelling and laterally flowing of the asthenospheric mantle and the crustal extension, producing the adakitic magmas during 25–12 Ma.

6.3. Relative contributions of mantle material input vs. the tectonic shortening to Tibetan crustal thickening

The Tibetan crust is twice as thick as average continental crust (60–80 km; Kind et al., 1996) with an abnormal thermal state that produces a weakened crust (e.g., Zhao et al., 1997). Our study on syn-collisional LVS and post-collisional Miocene adakitic rocks from southern Tibet provides new perspectives on when and how this softened and thickened crust formed. The ‘arc’ geochemical affinity (Fig. 5) of the Dianzhong andesites (LVS) formed during ~64–60 Ma (Zhou et al., 2004) suggests a magma source of mantle wedge with normal crustal thickness, or of recently formed oceanic basaltic crust at shallow depth. Absence of adakitic rocks in the LVS Dianzhong and Nianbo Formations also suggests that the crustal thickness in southern Tibet appears not to have reached 40–50 km prior to 50 Ma, which is inferred from experimental results on adakites (Rapp et al., 1991, 1999). We estimate that the crustal thickness was about 35 km at the time of Dianzhong andesite emplacement (64–60 Ma), and ~37 km when the Nianbo dacites were emplaced at ~54 Ma, roughly estimated by using the relationship of K_2O contents and Rb/Sr ratios of arc rocks with crustal thickness (Dickinson, 1971; Condie, 1982). Appearance of a few adakite-like rocks in the Pana rhyolitic succession with age of 50–40 Ma implies the presence of garnet as a residual phase in the source and the early stage of crustal thickening. Therefore, drastic collision-induced thickening (by ~20–30 km) of the Tibetan crust must have happened between the late stage of the Linzizong volcanism (after ~50 Ma) and the beginning of the Miocene adakitic magmatism (~25 Ma).

This drastic crustal thickening is often attributed to the tectonic thickening related to the Indian–Asian collision (e.g., Zhao et al., 1997). However, the following observations and inferences signify magmatic contributions. First, the absence of obvious deformation in the Tertiary LVS implies that upper crustal shortening contributed little to crustal thickening. Second, trace element and Sr–Nd isotope geochemistry of the Miocene adakitic rocks suggest that the input of more mafic magmas related to the Neo-Tethyan subduction and subsequent Indian–Asian collision during ~65–40 Ma appears to have produced a thickened juvenile lower crust. This process is also responsible for a thermally softened lithosphere. Third, the Moho in the Lhasa terrane is poorly defined (e.g., Zhao et al., 1997), which is consistent with continuous magmatic accretion due to magma piercing the Moho to contribute to the thickening of the lower crust.

An accurate assessment of the amount of magmatic addition to the crust is not straightforward. Volume estimation based on preserved volcanic rocks and outcrops of plutonic rocks (Kono et al., 1989) is often used, but this would underestimate it because mantle-derived magmas may be arrested at major density interfaces, e.g., mantle/crust interface (Petford and Atherton, 1996) and because of erosion of volcanic strata. The great thickness (~5 km) and widespread distribution of the LVS (with a few outcrops of mafic dykes) imply that a huge amount of the more mafic magmas was probably trapped at the base of south Tibetan lower crust. The crustal thickness is about 70 km on average in the Lhasa terrane. Assuming that the pre-collisional crust was ~35 km thick, and that the juvenile lower crust due to magmatic contribution is ∼15 km thick, as deduced from the seismic dada (∼14–20-km-thick layer of Vp = 7.2 km/s) beneath the Lhasa terrane (Owens and Zandt, 1997), the tectonic thickening should be about 20 km during the collision.

6.4. On the timing of the collision-induced crustal thickening of southern Tibet since ca. 65 Ma

The collisional and post-collisional igneous rocks provide useful constraints on the timing of the crustal thickening in the main collision zone. It is clear that the period of the LVS volcanism is one of the key periods for crustal growth and thickening since the onset of the Indian–Asian collision, and mantle input through magmatism is significant. We have done a simple exercise using Condie's (1982) equation, $C/\mathrm{km}=18.2\ K_{60}+0.45$, to estimate the crustal thickness, where C refers to thickness of the crust (km), and K_{60}, the K_2O content at 60 wt.% SiO_2. The equation K_{60}:$K_{SiO2}=60$: SiO_2 can be used to get K_{60} from the observed values at SiO_2 values other than 60 wt.%. The average values of related oxide contents analyzed for the LVS were used in the calculation as follows: SiO_2 60.50 wt.% and K_2O 1.89 wt.% for the Dianzhong volcanics, SiO_2 71.58 wt.% and K_2O 2.37 wt.% for the Nianbo volcanics, and SiO_2 74.17 wt.% and K_2O 5.25 wt.% for the Pana volcanics. The crustal thickness estimated by using Condie's equation is roughly 35 km, 37 km and 78 km during the periods of the Dianzhong (65–60 Ma), Nianbo (60–50 Ma) and Pana (50–40 Ma), respectively. It implies that the crustal thickness beneath southern Gangdese was probably still normal during the early–middle stage of the LVS eruption and had not significantly increased until the late Pana period (after 50 Ma).

The Miocene post-collisional igneous rocks also provide constraints on the timing of the crustal thickening. As Chung et al. (2003) and Hou et al. (2004) argued that the Miocene potassic adakitic rocks were originated from the lower portion of thickened crust, the crust beneath southern Tibet must have been thickened enough to allow producing potassic adakitic magmas (Rapp et al., 1999) before 25 Ma. Occurrence of post-collisional latitic and trachytic volcanics also suggest the magma source at the base of thickened crust in the same period of time (Wyllie, 1977). The magmatic gap between ∼40 Ma and 25 Ma does not allow estimation of the crustal thickness during this period, we infer that crustal thickening may have continued through continued tectonic compression.

7. Conclusions

1. The collisional and post-collisional igneous rocks in the Gangdese magmatic belt, especially the Paleogene Linzizong volcanic succession (LVS) and the Miocene adakitic rocks provide constraints on the crustal growth and thickening of the main collision zone in southern Tibet.
2. Three phases of collision-induced crustal thickening in southern Tibet are recognized: Phase I: formation of the juvenile crust during the period of ∼65–40 Ma, with major thickening of lower crust taking place at ∼50–40 Ma, by means of mantle-derived magma input. Phase II: crustal thickening as the result of tectonic shortening during the period of ca. 40–25 Ma, which coincides with a magmatic gap. Phase III: the period that retained the already thickened crust, yet associated with the thinning of the lithosphere since ∼25 Ma, which is interpreted as a response to asthenospheric upwelling and lateral flow as well as crustal extension while Indian–Asian convergence continued. Therefore, it seems that the collision-induced crustal thickening took place mainly in the period of ∼50 to ∼25 Ma, that is, the period between the late stage of the Linzizong volcanism and the beginning of the emplacement of adakitic rocks.
3. Most of the LVS rocks and the syn-collisional granitoids in the south Gangdese have positive ε_{Nd} values, emphasizing the significance of the mantle input for the crustal thickening. This idea is further supported by the study of the Miocene adakitic rocks. Two lines of evidence reveal that these potassic adakitic rocks were generated by the partial melting of a thickened mafic lower crust beneath southern Tibet. The crust beneath southern Tibet must have been considerably thickened before 25 Ma.
4. By assuming that the pre-collisional crust was ∼35 km thick, we estimated from both geochemical and seismic data that the input of mantle material has contributed about 40% (∼15 km in thickness) to the collision-induced net crustal thickening beneath the Lhasa terrane.

Acknowledgements

This study was supported by grants awarded under the National Key Project for Basic Research of China (Project 2002CB41260) from the Ministry of Science and Technology, China, the projects of the National Natural Science Foundation of China (Projects 40172025, 40103003, 40473020, 49802005 and

49772107) and the Key Project on the Tibetan Plateau, of the Ministry of Land and Resources of China (Project 2003009). We thank Su Zhou and Tang for assistance in $^{40}Ar/^{39}Ar$ age measurement and Sr–Nd isotope analysis. The authors benefited from the thorough review and constructive comments by Gregory Davis.

References

Altherton, M.P., Perford, N., 1993. Generation of sodium-rich magmas from newly underplated basaltic crust. Nature 362, 144–146.

Argand, E., 1924. La tectonique de asie. 13th International Geology Congress, vol. 7, p. 171.

Barharin, B., 1996. Genesis of the two main types of peraluminous granitoids. Geology 24, 295–298.

Ben Othman, D., Polve, M., Allegre, C.J., 1984. Nd-Sr isotopic composition of granulites and constraint on the evolution of the lower continental crust. Nature 307, 510–515.

Blinsiuk, P.M., Hacker, B., Glodny, J., Ratschbacher, L., Bill, S., Wu, Z.-H., McWilliams, M.O., Calvert, A., 2001. Normal faulting in central Tibet since at least 13.5 Myr ago. Nature 412, 628–632.

Chung, S.-L., Lo, C.-H., Lee, T.-Y., Zhang, Y.-Q., Xie, Y.-W., Li, X.-H., Wang, K.-L., Wang, P.-L., 1998. Dischronous uplift of the Tibetan plateau starting from 40 My ago. Nature 349, 769–773.

Chung, S.-L., Liu, D.-Y., Ji, J.-Q., Chu, M.-F., Lee, H.-Y., Wen, D.-J., Lo, C.-H., Lee, T.-Y., Yian, Q., Zhang, Q., 2003. Adakites from continental collision zone: melting of thicken lower-crust beneath southern Tibet. Geology 31, 1021–1024.

Coleman, M., Hodges, K., 1995. Evidence for Tibetan Plateau uplift before 14 Ma ago from a new minimum age for east–west extension. Nature 374, 49–52.

Condie, K.C., 1982. Plate Tectonics and Crustal Evolution. Pergamon, New York. 310 pp.

Copeland, P., Harrison, Y.M., Yun, P., 1995. Thermal evolution of the Gangdes batholith, Southern Tibet: a history of episodic unroofing. Tectonics 14, 223–236.

Coulon, C., Maluski, H., Bollinger, C., Wang, S., 1986. Mesozoic and Cenozoic volcanic rocks from central and southern Tibet: $^{39}Ar/^{40}Ar$ dating, petrological characteristics and geodynamic significance. Earth Planetary Science Letter 79, 281–302.

Defant, M.J., Drummond, M.S., 1990. Derivation of some modern arc magmas by melting of young subducted lithosphere. Nature 347, 662–665.

Defant, M.J., Kepezhinskas, P., 2001. Evidence suggests slab melting in arc magmas. EOS 82, 62–69.

Deng, W.-M., 1998. Cenozoic Intraplate Volcanic Rocks in the Northern Qinghai–Tibetan plateau. Ggeological Publishing House, Beijing. (in Chinese with English abstract).

Depaolo, D.J., 1985. Isotope studies of processes in mafic magma chambers: I. Kiglapait Intrusion, Labrador. Journal of Petrology 26, 925–951.

Depaolo, D.J., Perry, F.V., Baldridge, W.S., 1992. Crustal versus mantle sources of granitic magmas: a two-parameter model based on Nd isotopic studies. Royal Society of Edinburgh Transactions: Earth Sciences 83, 439–446.

Dewey, J.F., Bird, J.M., 1970. Mountain belts and new global tectonics. Journal of Geophyscial Research 74, 2625–2467.

Dickinson, W.R., 1971. Plate tectonics in geologic history. Science 174, 107–113.

Ding, L., Lai, Q.Z., 2003. Geological evidence for thickening and uplift of the Gangdese crust before collision—Constraints of arc convergence on the uplift and extension of the Qinghai–Tibetan plateau. Chinese Science Bulletin 48, 836–842 (in Chinese with English abstract).

Ding, L., Paul, K., Zhong, D., Deng, W., 2003. Cenozoic volcanism in Tibet; evidence for a transition from oceanic to continental subduction. Journal of Petrology 44 (10), 1833–1865.

Dong, G. C., 2002. Linzizong volcanic rocks in Linzhou Basin, Tibet and implications for India–Asia continental collision. Ph. D. Dissertation, China University of Geosciences, Beijing, 1–134.

Dong, Guochen, Mo, Xuanxue, Zhao, Zhidan, Guo, Tieying, Wang, Liangliang, Chen, Tao, 2005. Geochronologic constraints on the magmatic underplating of the Gangdise belt in the India–Eurasia collision: evidence of SHRIMP II zircon U–Pb dating. Acta Geologica Sinica 79 (6), 787–794.

Drummond, M.S., Defant, M.J., 1990. A model for trondhjemite–tonalite–dacite genesis and crustal growth via slab melting. Archean to modern comparisons. Journal of Geophyscial Research 95, 21503–21521.

Drummond, M.S., Defant, M.J., Kepezhinskas, P.K., 1996. Petrogenesis of slab-derived trondhjemite–tonalite–dacite/adakite magmas. Transactions of the Royal Society of Edinburgh, Earth Sciences 87, 205–215.

Durr, S.B., 1996. Provenance of Xigaze fore-arc basin clastic rocks (Cretaceous, south Tibet). Geological Society of America Bulletin 108, 669–684.

England, P.C., Houseman, G.A., 1989. Extension during continental convergence with application to the Tibetan Plateau. Journal of Geophyscial Research 94, 17561–17579.

Flower, M., Russo, R., Tamaki, K., Nguyen, H., 2001. Mantle contamination and the Izu–Bonin–Mariana (IBM) 'high-tide mark'; evidence for mantle extrusion caused by Tethyan closure. Tectonophysics 333, 9–34.

Garzione, C.N., DeCelles, P.G., Ojha, T.P., Upreti, B.N., 2003. East–west extension and Miocene environmental change in the southern Tibetan plateau: Thakkhola graben, central Nepal. Geological Society of America Bulletin 115, 3–20.

Gou, Z., Wilson, M., Liu, J., 2007. Post-collisional adakites in south Tibet: products of partial melting of subduction-modified lower crust. Lithos 96, 205–224 (this issue). doi:10.1016/j.lithos.2006.09.011.

Harrison, T.M., Copeland, P., Kidd, W.S.F., Yin, A., 1992. Raising Tibet. Science 255, 1663–1670.

Hou, Z.-Q., Ma, H.-W., Zaw, K., Zhang, Y.-Q., Wang, M.-J., Wang, Z., Pan, G.-T., Tang, R.-L., 2003. The Himalayan Yulong porphyry copper belt: produced by large-scale strike–slip faulting at Eastern Tibet. Economic Geology 98, 125–145.

Hou, Z.-Q., Gao, Y.-F., Qu, X.-M., Rui, Z.-Y., Mo, X.-X., 2004. Origin of adakitic intrusives generated during mid-Miocene east–west extension in South Tibet. Earth Planetary Science Letter 220, 139–155.

Kapp, P., Guynn, J.H., 2004. Indian punch rifts Tibet. Geology 32 (11), 993–996.

Kay, R.W.J., 1978. Aleutian magnesium andesites; melts from subducted Pacific oceanic crust. Journal of Volcano and Geothermal Research 4, 117–132.

Kay, S.M., Ramos, V.A., Marquez, M., 1993. Evidence in Cerro Pampa volcanic rocks for slab-melting prior to ridge-trench collision in Southern South America. Journal of Geology 101, 703–714.

Kind, R., Ni, J., Zhao, W., Wu, J., Yuan, X., Zhao, L., Sandvol, E., Reese, C., Nabelek, J., Hearn, T., 1996. Evidence from earthquake data for partially molten crustal layer in Southern Tibet. Science 274, 1692–1694.

Kono, M., Fukao, Y., Yamamoto, A., 1989. Mountain building in the central Andes. Journal of Geophyscial Research 94, 3891–3905.

Maheo, G., Guillot, S., Blichert-Tofa, J., Rolland, Y., Pecher, A., 2002. A slab break-off model for the Neogene thermal evolution of Southern Karakorum and South Tibet. Earth Planetary Science Letter 195, 45–58.

Mahoney, J.J., Frei, R., Tejada, M.L.G., Mo, X.X., Leat, P.T., 1998. Tracing the Indian ocean mantle domain through time: isotopic results from old west Indian, east Tethyan and south Pacific seafloor. Journal of Petrology 39, 1285–1306.

Maluski, H., Proust, F., Xiao, X.C., 1982. $^{39}Ar/^{40}Ar$ dating of the trans-Himalayan calc-alkaline magmatism of southern Tibet. Nature 298, 152–156.

Martin, H., 1986. Effect of steeper Archean geothermal gradient on geochemistry of subduction zone magmas. Geology 14, 753–756.

Mcdonough, W.F., Sun, S.S., Ringwood, A.E., Jagoutz, E., Hoffmann, A.W., 1991. K, Rb and Cs in the Earth and Moon and the evolution of the Earth's mantle. Geochim. Cosmochim. Acta, Ross Taylor Symposium Volume.

Miller, C., Schuster, R., Klotzli, U., Frank, W., Purtscheller, F., 1999. Post-collisional potassic and ultrapotassic magmatism in SW Tibet; geochemical and Sr–Nd–Pb–O isotopic constraints for mantle source characteristics and petrogenesis. Journal of Petrology 40 (9), 1399–1424.

Mo, X.-X., Zhao, Z.-D., Deng, J.-F., Dong, G.-C., Zhou, S., Guo, T.-Y., Zhang, S.-Q., Wang, L.-L., 2003. Response of volcanism to the India–Asian collision. Earth Science Frontiers 10, 135–148 (Chinese with English abstract).

Mo, Xuanxue, Dong, Guochen, Zhao, Zhidan, Guo, Tieying, Wang, Liangliang, Chen, Tao, 2005a. Timing of magma mixing in the Gangdise magmatic belt doring the India–Asia collision: zircon SHRIMP U–Pb dating. Acta Geologica Sinica 79, 66–76.

Mo, X., Dong, Z., Zhou, Z., Zhou, S., Wang, L., Qiu, R., Zhang, F., 2005b. Spatial and temporal distribution and characteristics of granitoids in the Gangdese, Tibet and implication for crustal growth and evolution. Geological Journal, China University 11, 281–290 (in Chinese with English abstract).

Mo, X., Zhao, Z., Deng, J., Flower, M., Yu, X., Luo, Z., Li, Y., Zhou, S., Dong, G., Zhu, D., Wang, L., 2006. Petrology and geochemistry of post-collisional volcanic rocks from the Tibetan Plateau: implications for lithosphere heterogeneity and collision-induced asthenospheric mantle flow. In: Dilek, Yildirim, Pavlides, Spyros (Eds.), Postcollisional Tectonics and Magmatism in the Mediterranean Region and Asia. Geological Society of America Special Paper 409, pp. 507–530. doi:10.1130/2006.2409(24).

Molnar, P., Houseman, G., Clinton, C., 1998. Rayleigh–Taylor instability and convective thinning of mechanically thickened lithosphere; effects of non-linear viscosity decreasing exponentially with depth and of horizontal shortening of the layer. Geophysical Journal International 133, 568–584.

Murphy, M.A., Yin, A., Harrison, T.M., Durr, S.B., Chen, Z., Ryerson, F.J., Kidd, W.S.F., Wang, X., Zhou, X., 1997. Significant crustal shorting in south-central Tibet prior to the Indo–Asian collision. Geology 25, 719–722.

Nelson, K.D., Zhao, W.-J., Brown, L.D., Kuo, J., Che, J.-K., Liu, X.-W., Klemperer, S.L., Makovsky, Y., Meissner, R., Mechie, J., Kind, R., Wenzel, F., Ni, J., Nabelek, J., Chen, L.-S., Tan, T.-D., Wei, W.-B., Jones, A.G., Booker, J., Unsworth, M., Kidd, W.S.F., Hauck, M., Alsdorf, D., Ross, A., Cogan, M., Wu, C.-D., Sandvol, E., Edwards, M., 1996. Partial molten middle crust beneath Southern Tibet: synthesis of Project INDEPTH results. Science 274, 1684–1688.

Niu, Y., 2005. Generation and evolution of basaltic magmas: some basic concepts and a hypothesis for the origin of the Mesozoic–Cenozoic volcanism in eastern China. Geological Journal. China University 11, 9–46.

Owens, T.J., Zandt, G., 1997. Implications of crustal property variations for models of Tibetan plateau evolution. Nature 387, 37–43.

Peacock, S.M., 2003. Thermal structure and metamorphic evolution of subducting slabs. Inside the Subduction Factory. Geophys. Monogr., vol. 238, pp. 7–22.

Perry, F.V., Depaolo, D.J., Baldridge, W.S., 1993. Neodymium isotopic evidence for decreasing crustal contributions to Cenozoic ignimbrites of the western United States: implications for the thermal evolution of the Cordilleran crust. Geological Society of America Bulletin 105, 872–882.

Petford, N., Atherton, M., 1996. Na-rich partial melts from newly underplated basaltic crust: the Cordillera Blanca bathloith, Peru. Journal of Petrology 37, 1491–1521.

Powell, C.M., 1986. Continental underplating model for the rise of the Tibetan plateau. Earth Planetary Science Letter 81, 79–94.

Qu, X.M., Hou, Z.-Q., Li, Z.Q., 2003. $^{40}Ar/^{39}Ar$ ages of porphyries from the Gangdese porphyry Cu belt in south Tibet and implication to geodynamic setting. Acta Geologica Sinica 77, 245–252 (in Chinese with English abstract).

Rapp, R.P., Watson, E.B., Miller, C.F., 1991. Partial melting of amphibolite/eclogite and the genesis of Archean trondjemites and tonalites. Precambrian Research 51, 1–25.

Rapp, P.R., Shimizu, N., Norman, M.D., Applegate, G.S., 1999. Reaction between slab-derived melt and peridotite in the mantle wedge: experimental constrains at 3.8 Gpa. Chemical Geology 160, 335–356.

Rudnick, R.L., Fountain, D.M., 1995. Nature and composition of the continental crust: a lower crustal perspective. Review in Geophysics 33, 267–309.

Rui, Z.-Y., Li, G.-M., Zhang, L.-S., Wang, L.-S., 2004. The response of porphyry copper deposits to important geological events in Xizang (Tibet). Earth Science Frontiers 11, 145–152 (Chinese with English abstract).

Schärer, E., Xu, R.-H., Allegere, C.J., 1984. U–Pb geochronology of the Gangdese (Transhimalaya) plutonism in the Lhasa-Xizang region, Tibet. Earth Planetary Science Letter 69, 311–320.

Schmitz, M., 1994. A balanced model of the southern central Andes. Tectonics 13, 484–492.

Stern, C.R., Kilian, R., 1996. Role of the subducted slab, mantle wedge and continental crust in the generation of adakites from the Andean Austral Volcanic Zone. Contribution Mineralogy and Petrology 123, 263–281.

Sylvester, P.J., 1998. Post-collision strongly peraluminous granites. Lithos 45, 29–44.

Tatsumi, Y., 1986. Chemical characteristics of fluid phase released from a subduction lithosphere and origin of arc magma: evidence from high-pressure experiments and natural rocks. Journal of Volcano and Geothermal Research 29, 293–309.

Turner, S., Hawkesworth, G., Liu, J., Rogers, N., Kelley, S., Calsteren, P.V., 1993. Timing of Tibetan uplift constrained by analysis of volcanic rocks. Nature 364, 50–54.

Williams, H., Turner, S., Kelley, S., Harris, N., 2001. Age and composition of dikes in Southern Tibet: new constraints on the timing of east–west extension and its relationship to post-collisional volcanism. Geology 29, 339–342.

Wyllie, P.J., 1977. Crustal anatexis; an experimental review. Tectonphysics 43, 41–71.

Xu, J.F., Shinjo, R., Defant, M.J., Wang, Q., Rapp, R.P., 2002. Origin of Mesozoic adakitic intrusive rocks in the Ningzhen area of east

China: partial melting of delaminated lower continental crust? Geology 30, 1111–1114.

Yin, A., Harrison, T., 2000. Geologic evolution of the Himalayan–Tibetan orogen. Annual Review of Earth and Planetary Sciences 28, 211–280.

Yin, A., Kapp, P.A., Murphy, M.A., Harrison, T.M., Grove, M., Ding, L., Deng, X., Wu, C., 1999. Significant late Neogene east–west extension in northern Tibet. Geology 27, 787–790.

Zhang, Q.-S., 2005. unpub. PhD dissertation. China University of Mining, Beijing, 120 pp. (in Chinese).

Zhao, W.L., Morgen, W.J., 1987. Injection of Indian crust into Tibetan lower crust: a two-dimensional finite element model study. Tectonics 6, 489–504.

Zhao, W.-J., Nelson, K.D., Meissner, R., 1997. Advances of INDEPTH deep profiling study in Tibet and the Himalayas. Episodes 20, 266–272.

Zhao, Z.-D., Mo, X.-X., Zhang, S.-Q., Guo, T.-Y., Zhou, S., Dong, G.-C., Wang, Y., 2001. Post-collisional magmatisms in Wuyu basin, middle Tibet. Science in China 31, 20–26 (in Chinese).

Zhou, S., Mo, X.-X., Dong, G.-C., Zhao, Z.-D., Qiu, R.-Z., Guo, T.-Y., Wang, L.-L., 2004. ^{40}Ar-^{39}Ar geochronology of Cenozoic Linzizong volcanic rocks from Linzhou Basin, Tibet, China, and their geological implications. Chinese Science Bulletin 49, 1970–1979.

Zindler, A., Hart, S.R., 1986. Chemical geodynamics. Annual Review of Earth and Planetary Sciences 14, 493–571.